PROCEEDINGS, Twenty-Ninth Workshop on Geothermal Reservoir Engineering
Stanford University, Stanford, California, January 26-28, 2004
SGP-TR-175

UNIVERSAL CAPILLARY PRESSURE AND RELATIVE PERMEABILITY MODEL FROM FRACTAL CHARACTERIZATION OF ROCK

Kewen Li and Roland N. Horne

Stanford Geothermal Program, Stanford University
Green Earth Science Building, 367 Panama St.
Stanford, CA 94305-2220, USA
e-mail: kewenli@stanford.edu

ABSTRACT

Capillary pressure and relative permeability are important parameters in geothermal reservoir engineering. It is essential to represent capillary pressure curves mathematically in an appropriate way. The Brooks-Corey capillary pressure model has been accepted widely, however it has been found that the Brooks-Corey model cannot represent capillary pressure curves of The Geysers rock samples. In fact, few existing capillary pressure models work for these rock samples. To this end, the porous media were modeled using fractal geometry and a universal capillary pressure model was derived theoretically. It was found that the universal capillary pressure model could be reduced to the frequently-used Brooks-Corey capillary pressure model and the Li-Horne imbibition model when the fractal dimension of the porous media takes a limiting value. This also demonstrates that the Brooks-Corey model and the Li-Horne model, which have been considered to be empirical, have a solid theoretical base. The results demonstrated that the new capillary pressure model could represent the capillary pressure curves of The Geysers rock while the Brooks-Corey model cannot. A relative permeability model was also developed from the universal capillary pressure model. Fractal dimension, a parameter associated with the heterogeneity of the rock, determines the shape of relative permeability curves according to the new relative permeability model. The new model can also be reduced to the Brooks-Corey relative permeability model. The relative permeability data of The Geysers rock were calculated using the typical values of the fractal dimension inferred from the mercury intrusion capillary pressure curves.

INTRODUCTION

Experimental data showed that the capillary pressure curves of rock samples with many fractures (The Geysers rock) were different from those of rock samples without fractures (for example, Berea sandstone). It was found that the Brooks-Corey (1964) capillary pressure model could be used to represent the curves of the rock without fractures but did not work for The Geysers rock samples with many fractures (Li and Horne, 2003). For example, Fig. 1 shows that the capillary pressure curve of Berea sandstone is a straight line on a log-log plot, which implies that the Brooks-Corey capillary pressure model works for Berea sandstone. However the capillary pressure curves of The Geysers rock are not straight lines, which demonstrates that the Brooks-Corey capillary pressure model does not work for The Geysers rock. The capillary pressure curves were measured using a mercury intrusion technique. It would be helpful for reservoir engineers to have a mathematical model to represent such capillary pressure curves appropriately.

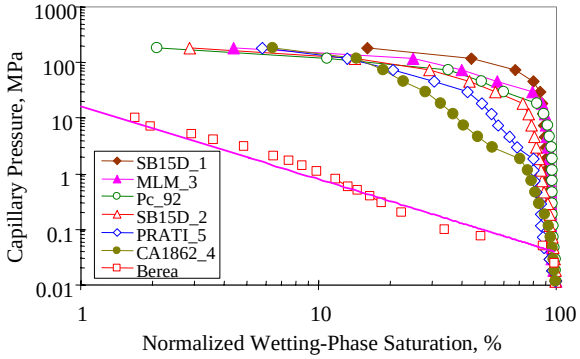

Figure 1: Capillary pressure curves of The Geysers rock and Berea sandstone.

In Fig. 1, the open squares represent the capillary pressure data of Berea sandstone. All the other symbols represent the capillary pressure curves of The Geysers rock from different wells.

Interestingly, Li and Horne (2003) found that fractal curves inferred from capillary pressure curves were good straight lines for all the rock samples, both those with and those without fractures, as shown in Fig. 2. The fractal curves represent the relationship

between the number of pores and the radius of the pore throats.

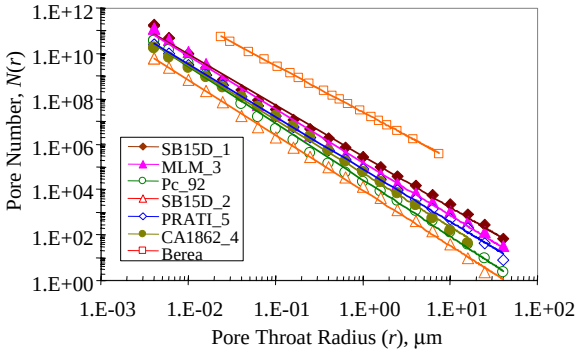

Figure 2: Fractal Curves of The Geysers rock and Berea sandstone.

This finding implies that a general capillary pressure model may exist to represent both the rock in which the Brooks-Corey model works and the rock in which the Brooks-Corey model does not work. In this study, such a general capillary pressure model was derived theoretically from fractal modeling of porous media. A general relative permeability model was also developed based on the universal capillary pressure model. Experimental data of capillary pressure from The Geysers rock were used to test the new capillary pressure and relative permeability model.

THEORY

According to the basic concept of fractal geometry, the following expression applies to a fractal object:

$$N(r) \propto r^{-D_f} \tag{1}$$

where r is the radius (or characteristic length) of a unit chosen to fill the fractal object, $N(r)$ is the number of the units (with a radius of r) required to fill the entire fractal object, and D_f is the so-called fractal dimension. The fractal dimension is a representation of the heterogeneity of the fractal object. The greater the fractal dimension, the more heterogeneous the fractal object.

Capillary pressure curves measured by a mercury-intrusion technique are often used to infer the pore size distribution of rock samples. In making this inference, rock with solid skeleton and pores is represented by using a capillary tube model. $N(r)$ can be calculated easily once capillary pressure curves measured using a mercury-intrusion technique are available. The unit chosen in this study was a cylindrical capillary tube with a radius of r and a length of l. So the volume of the unit is equal to $\pi r^2 l$ and $N(r)$ at a given radius of r is then calculated easily.

A universal capillary pressure model

Once $N(r)$ is known, the value of fractal dimension, D_f, can be determined from the relationship between $N(r)$ and r. The relationship between $N(r)$ and r should be linear on a log-log plot if the pore system of the rock is fractal.

According to the capillary tube model, $N(r)$ can be calculated as follows:

$$N(r) = \frac{V_{Hg}}{\pi r^2 l} \tag{2}$$

where l is the length of a capillary tube and V_{Hg} is the cumulative volume of mercury intruded in the rock sample when capillary pressure is measured.

Combining Eq. 1 and Eq. 2:

$$\frac{V_{Hg}}{\pi r^2 l} \propto r^{-D_f} \tag{3}$$

Arranging Eq. 3:

$$V_{Hg} \propto r^{2-D_f} \tag{4}$$

Considering a capillary tube model, capillary pressure can be calculated as follows:

$$P_c = \frac{2\sigma \cos\theta}{r} \tag{5}$$

where P_c is the capillary pressure, σ is the surface tension, and θ is the contact angle.

Substituting Eq. 5 into Eq. 4:

$$V_{Hg} \propto P_c^{-(2-D_f)} \tag{6}$$

The mercury saturation is calculated as follows:

$$S_{Hg} = \frac{V_{Hg}}{V_p} \tag{7}$$

where S_{Hg} is the mercury saturation and V_p is the pore volume of the core sample.

Substituting Eq. 7 into Eq. 6:

$$S_{Hg} = aP_c^{-(2-D_f)} \tag{8}$$

here a is a constant.

When V_{Hg} increases from 0 to 0^+, the corresponding capillary pressure increases from 0 to p_e. According to Eq. 8:

$$S_{Hg}(V_{Hg} \to 0) = \varepsilon = a p_e^{-(2-D_f)} \tag{9}$$

where ε is an infinite small positive value close to zero and p_e is the entry capillary pressure of the rock sample.

Similarly the capillary pressure reaches a maximum value (it can also be infinite) when V_{Hg} equals a maximum value. According to Eq. 8:

$$S_{Hg,\max} = a P_{c,\max}^{-(2-D_f)} \tag{10}$$

where $S_{Hg,\max}$ is the maximum mercury saturation and $P_{c,\max}$ is the maximum capillary pressure at $S_{Hg,\max}$.

Combining Eqs. 8, 9, and 10, one can obtain:

$$\frac{S_{Hg} - \varepsilon}{S_{Hg,\max} - \varepsilon} = \frac{P_c^{-(2-D_f)} - p_e^{-(2-D_f)}}{P_{c,\max}^{-(2-D_f)} - p_e^{-(2-D_f)}} \tag{11}$$

Considering $\varepsilon \to 0$, Eq. 11 may be reduced to:

$$\frac{S_{Hg}}{S_{Hg,\max}} \approx \frac{P_c^{-(2-D_f)} - p_e^{-(2-D_f)}}{P_{c,\max}^{-(2-D_f)} - p_e^{-(2-D_f)}} \tag{12}$$

Using the wetting-phase saturation (the wetting-phase during mercury intrusion is air), Eq. 12 can be expressed as:

$$\frac{1 - S_w}{1 - S_{wr}} = \frac{P_c^{-(2-D_f)} - p_e^{-(2-D_f)}}{P_{c,\max}^{-(2-D_f)} - p_e^{-(2-D_f)}} \tag{13}$$

where S_w is the wetting-phase saturation and S_{wr} is the residual saturation of the wetting-phase.

Eq. 13 can be rearranged as:

$$\frac{1 - S_w}{1 - S_{wr}} = 1 - \frac{P_{c,\max}^{-(2-D_f)} - P_c^{-(2-D_f)}}{P_{c,\max}^{-(2-D_f)} - p_e^{-(2-D_f)}} \tag{14}$$

The normalized wetting-phase saturation is defined as:

$$S_w^* = \frac{S_w - S_{wr}}{1 - S_{wr}} \tag{15}$$

Substituting Eq. 15 into Eq. 14:

$$S_w^* = \frac{P_{c,\max}^{-(2-D_f)} - P_c^{-(2-D_f)}}{P_{c,\max}^{-(2-D_f)} - p_e^{-(2-D_f)}} \tag{16}$$

Arranging Eq. 16:

$$P_c = [P_{c,\max}^{-\lambda} - (P_{c,\max}^{-\lambda} - p_e^{-\lambda}) S_w^*]^{-\frac{1}{\lambda}} \tag{17}$$

where $\lambda = 2 - D_f$.

Eq. 17 can be reduced as follows:

$$P_c = P_{c,\max}(1 - b S_w^*)^{-\frac{1}{\lambda}} \tag{18}$$

where b is a constant and expressed as follows:

$$b = 1 - \left(\frac{p_e}{P_{c,\max}}\right)^{-\lambda} \tag{19}$$

For $D_f<2$, if $P_{c,\max}$ approaches infinity, then Eq. 17 or 18 can be reduced:

$$P_c = p_e (S_w^*)^{-\frac{1}{\lambda}} \tag{20a}$$

Eq. 20a is the frequently-used Brooks-Corey model, which was proposed empirically by Brooks and Corey (1964).

According to the derivation in this paper, one can see that the Brooks-Corey capillary pressure model has a solid theoretical basis. This may be why the Brooks-Corey model can be a good fit to capillary pressure curves of many rock samples.

In the case in which b=1, Eq. 18 can be reduced to:

$$P_c = P_{c,\max}(1 - S_w^*)^{-\frac{1}{\lambda}} \tag{20b}$$

Eq. 20b is the imbibition capillary pressure model proposed by Li and Horne (2001) empirically (for $D_f>2$).

In the case in which b=0, Eq. 18 can be reduced as:

$$P_c = P_{c,\max} \tag{20c}$$

Eq. 20c may be considered a capillary pressure model for a single capillary tube.

One can see that Eq. 18, as a general capillary pressure model, could be applied in both complicated

porous media and in a single capillary tube as well as in both drainage and imbibition cases.

Differentiating Eq. 16:

$$\frac{dS_w^*}{dP_c} \propto -P_c^{-(3-D_f)} \tag{21}$$

Eq. 21 can also be expressed as:

$$\frac{dS_{Hg}}{dP_c} \propto P_c^{-(3-D_f)} \tag{22}$$

Eq. 22 is similar to the equation derived by Friesen and Mikula (1987):

$$\frac{dS_{Hg}}{dP_c} \propto P_c^{-(4-D_f)} \tag{23}$$

Note that the same equation could be obtained if a three-dimensional pore model, instead of a two-dimensional capillary tube model, were used to calculate the number of pores in the porous media.

A new relative permeability model

There are two main ways to infer relative permeability from capillary pressure data. One is the Purcell approach (1949) and another is the Burdine approach (1953). In this section, relative permeability models will be derived theoretically based on the new capillary pressure model (Eq. 18) using both the Purcell and the Burdine approaches.

Based on the Purcell approach

Purcell (1949) developed an equation to compute rock permeability by using capillary pressure data. This equation can be extended readily to the calculation of multiphase relative permeability. In two-phase flow, the relative permeability of the wetting phase can be calculated as follows:

$$k_{rw} = \frac{\int_0^{S_w} dS_w/(P_c)^2}{\int_0^1 dS_w/(P_c)^2} \tag{24}$$

where k_{rw} and S_w are the relative permeability and saturation of the wetting phase; P_c is the capillary pressure as a function of S_w.

Similarly, the relative permeability of the nonwetting phase can be calculated as follows:

$$k_{rnw} = \frac{\int_{S_w}^1 dS_w/(P_c)^2}{\int_0^1 dS_w/(P_c)^2} \tag{25}$$

where k_{rnw} is the relative permeability of the nonwetting phase. It can be seen from Eqs. 24 and 25 that the sum of the wetting and nonwetting phase relative permeabilities at a specific saturation is equal to one. This may not be true in most porous media. Comparing the experimental data with the modeling data, Li and Horne (2002) found that the Purcell model (Eqs. 24 and 25) may be the best fit to the experimental data of the wetting phase relative permeability for both drainage and imbibition processes but may not be a good fit for the nonwetting phase.

Substituting Eq. 18 into Eq. 24:

$$k_{rw} = \frac{\int_0^{S_w^*} [P_{c,\max}{}^{-\lambda} - (P_{c,\max}{}^{-\lambda} - p_e^{-\lambda})S_w^*]^{\frac{2}{\lambda}} dS_w^*}{\int_0^1 [P_{c,\max}{}^{-\lambda} - (P_{c,\max}{}^{-\lambda} - p_e^{-\lambda})S_w^*]^{\frac{2}{\lambda}} dS_w^*} \tag{26}$$

Defining:

$$S_{we} = P_{c,\max}{}^{-\lambda} - (P_{c,\max}{}^{-\lambda} - p_e^{-\lambda})S_w^* \tag{27}$$

one can obtain:

$$dS_w^* = -\frac{1}{P_{c,\max}{}^{-\lambda} - p_e^{-\lambda}} dS_{we} \tag{28}$$

Substituting Eqs. 27 and 28 into Eq. 26:

$$k_{rw} = \frac{\int_\beta^{S_{we}} (S_{we})^{\frac{2}{\lambda}} dS_{we}}{\int_\beta^\alpha (S_{we})^{\frac{2}{\lambda}} dS_{we}} \tag{2.29}$$

where:

$$\beta = P_{c,\max}^{-\lambda} \tag{30}$$

$$\alpha = p_e^{-\lambda} \tag{31}$$

After integrating:

$$k_{rw} = \frac{(S_{we})^{\frac{2+\lambda}{\lambda}} - \beta^{\frac{2+\lambda}{\lambda}}}{\alpha^{\frac{2+\lambda}{\lambda}} - \beta^{\frac{2+\lambda}{\lambda}}} \tag{32}$$

Eq. 32 can be expressed as:

$$k_{rw} = \frac{[P_{c,\max}{}^{-\lambda} - (P_{c,\max}{}^{-\lambda} - p_e^{-\lambda})S_w^*]^{\frac{2+\lambda}{\lambda}} - (P_{c,\max})^{-(2+\lambda)}}{(p_e)^{-(2+\lambda)} - (P_{c,\max})^{-(2+\lambda)}} \quad (33)$$

According to Eq. 25, the relative permeability of the nonwetting phase can be calculated as follows:

$$k_{rnw} = \frac{\alpha^{\frac{2+\lambda}{\lambda}} - (S_{we})^{\frac{2+\lambda}{\lambda}}}{\alpha^{\frac{2+\lambda}{\lambda}} - \beta^{\frac{2+\lambda}{\lambda}}} \quad (34)$$

Eq. 34 can also be expressed as:

$$k_{rnw} = \frac{(P_e)^{-(2+\lambda)} - [P_{c,\max}{}^{-\lambda} - (P_{c,\max}{}^{-\lambda} - p_e^{-\lambda})S_w^*]^{\frac{2+\lambda}{\lambda}}}{(p_e)^{-(2+\lambda)} - (P_{c,\max})^{-(2+\lambda)}} \quad (35)$$

According to Eq. 33:

$$k_{rw}(S_w^* = 0) = 0 \quad (36)$$

and

$$k_{rw}(S_w^* = 1) = 1 \quad (37)$$

According to Eq. 35:

$$k_{rnw}(S_w^* = 0) = 1 \quad (38)$$

and

$$k_{rnw}(S_w^* = 1) = 0 \quad (39)$$

The previous results of end-point relative permeability for both wetting phase and nonwetting phase show, to some extent, the validity of the new relative permeability model.

One can see from Eqs. 33 and 35 that relative permeability depends not only upon the heterogeneity (represented by fractal dimension through the parameter λ) but also upon the pore size of porous media, represented by the entry capillary pressure and the maximum capillary pressure, in some cases.

when D_f<2 and $P_{c,\max}$ approaches infinity, Eqs. 33 and 35 can be reduced to the simple Purcell relative permeability model expressed as follows:

$$k_{rw} = (S_w^*)^{\frac{2+\lambda}{\lambda}} \quad (40)$$

$$k_{rnw} = 1 - (S_w^*)^{\frac{2+\lambda}{\lambda}} \quad (41)$$

Therefore the new relative permeability model (Eqs. 33 and 35) encompasses the Purcell relative permeability model (Eqs. 40 and 41).

In cases where $P_{c,\max}$ has a finite value, Eqs. 33 and 35 can be reduced as follows:

$$k_{rw} = \frac{(1 - bS_w^*)^m - 1}{(1-b)^m - 1} \quad (42)$$

$$k_{rnw} = \frac{(1-b)^m - (1 - bS_w^*)^m}{(1-b)^m - 1} \quad (43)$$

where b is defined in Eq. 19 and m is expressed as follows:

$$m = \frac{2+\lambda}{\lambda} = \frac{4 - D_f}{2 - D_f} \quad (44)$$

Note that m is a parameter associated with the heterogeneity of the porous media because the fractal dimension D_f is a representation of heterogeneity. Parameter b is associated with the size of the pore in porous media.

Based on the Burdine model

Burdine (1953) developed equations similar to Purcell's method by introducing a tortuosity factor as a function of wetting phase saturation. The relative permeability of the wetting phase can be computed as follows:

$$k_{rw} = (\lambda_{rw})^2 \frac{\int_0^{S_w} dS_w/(P_c)^2}{\int_0^1 dS_w/(P_c)^2} \quad (45)$$

where λ_{rw} is the tortuosity ratio of the wetting phase. According to Burdine (1953), λ_{rw} could be calculated as follows:

$$\lambda_{rw} = \frac{\tau_w(1.0)}{\tau_w(S_w)} = \frac{S_w - S_m}{1 - S_m} \quad (46)$$

where S_m is the minimum wetting phase saturation from the capillary pressure curve; $\tau_w(1.0)$ and $\tau_w(S_w)$ are the tortuosities of the wetting phase when the wetting phase saturation is equal to 100% and S_w respectively.

In the same way, relative permeabilities of the nonwetting phase can be calculated by introducing a

tortuosity ratio of the nonwetting phase. The equation can be expressed as follows:

$$k_{rnw} = (\lambda_{rnw})^2 \frac{\int_{S_w}^{1} dS_w/(P_c)^2}{\int_0^1 dS_w/(P_c)^2} \quad (47)$$

where λ_{rnw} is the tortuosity ratio of the nonwetting phase, which can be calculated as follows:

$$\lambda_{rnw} = \frac{\tau_{nw}(1.0)}{\tau_{nw}(S_w)} = \frac{1-S_w-S_e}{1-S_m-S_e} \quad (48)$$

Here S_e is the equilibrium saturation of the nonwetting phase; τ_{nw} is the tortuosity of the nonwetting phase.

Using a similar procedure to that used to derive Eqs. 33 and 35, one can obtain:

$$k_{rw} = \frac{(S_{we})^{\frac{2+\lambda}{\lambda}} - \beta^{\frac{2+\lambda}{\lambda}}}{\alpha^{\frac{2+\lambda}{\lambda}} - \beta^{\frac{2+\lambda}{\lambda}}} (S_w^*)^2 \quad (49)$$

$$k_{rnw} = \frac{\alpha^{\frac{2+\lambda}{\lambda}} - (S_{we})^{\frac{2+\lambda}{\lambda}}}{\alpha^{\frac{2+\lambda}{\lambda}} - \beta^{\frac{2+\lambda}{\lambda}}} (1-S_w^*)^2 \quad (50)$$

when D_f<2 and $P_{c,\max}$ approaches infinity, Eqs. 49 and 50 can be reduced to the simple Brooks-Corey relative permeability model. The model is expressed as follows:

$$k_{rw} = (S_w^*)^{\frac{2+3\lambda}{\lambda}} \quad (51)$$

$$k_{rnw} = (1-S_w^*)^2[1-(S_w^*)^{\frac{2+\lambda}{\lambda}}] \quad (52)$$

Therefore the new relative permeability model (Eqs. 49 and 50) encompasses the Brooks-Corey relative permeability model (Eqs. 51 and 52).

In the case in which $P_{c,\max}$ has a finite value, Eqs. 49 and 50 can be reduced as follows:

$$k_{rw} = \frac{(S_w^*)^2[(1-bS_w^*)^m - 1]}{(1-b)^m - 1} \quad (53)$$

$$k_{rnw} = \frac{(1-S_w^*)^2[(1-b)^m - (1-bS_w^*)^m]}{(1-b)^m - 1} \quad (54)$$

In the case in which b=1 and m>0, Eqs. 53 and 54 can be reduced as follows:

$$k_{rw} = (S_w^*)^2[1-(1-S_w^*)^m] \quad (55)$$

$$k_{rnw} = (1-S_w^*)^{2+m} \quad (56)$$

In the case in which m=0, Eqs. 55 and 57 can be reduced as follows:

$$k_{rw} = (S_w^*)^2 \quad (57)$$

$$k_{rnw} = (1-S_w^*)^2 \quad (58)$$

Eqs. 57 and 58 are the relative permeability model in a single capillary tube.

Eqs. 51 and 52 have been tested against experimental data in many cases (Li and Horne, 2002). However the new relative permeability models developed in this study are yet to be verified.

RESULTS

The theoretical capillary pressure data were calculated using Eq. 18 with different values of fractal dimension and the results are shown in Fig. 3. The values of fractal dimension used in the calculation were 1.0, 2.1, and 2.8. The values of maximum capillary pressure and entry capillary pressure were 100 MPa and 0.4 MPa respectively in all of the cases. The residual wetting-phase saturation was 20%. For D_f<2.0, the capillary pressure curve looks like the often-observed capillary pressure curve (for example, the capillary pressure curve of Berea sandstone). This type of capillary pressure curve can usually be represented mathematically by the Brooks-Corey model. For D_f>2.0, the capillary pressure curve is concave to the axis of the wetting-phase saturation. The capillary pressure curves of The Geysers rock have such a feature.

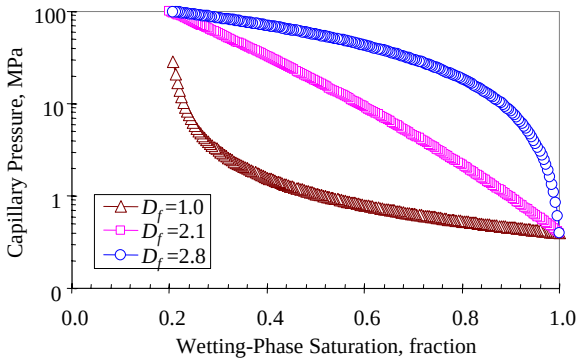

Figure 3: Typical capillary pressure curves calculated using the new model with different values of fractal dimension.

A typical capillary pressure curve of The Geysers rock is shown in Fig. 4. It is obvious that the Brooks-Corey model cannot represent such a capillary pressure curve. The new capillary pressure model developed in this study was used to match the data and the results are demonstrated in Fig. 4. One can see that the new capillary pressure model can represent the capillary pressure curve of The Geysers rock satisfactorily. The values of parameters obtained by the match were: $P_{c,\,max}$=198.8 MPa, b=0.999, and λ=0.65. The value of fractal dimension calculated using the value of λ was 3.538.

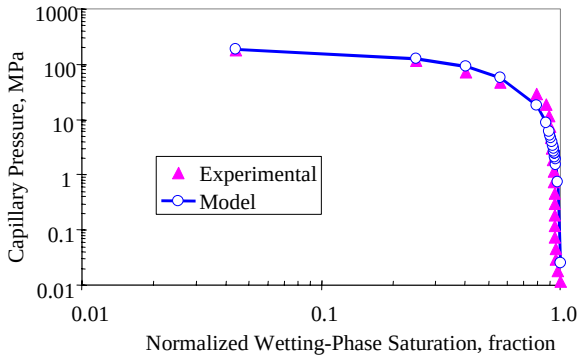

Figure 4: Typical capillary pressure curve of The Geysers rock and the match by using the universal model..

Relative permeability curves were calculated according to the new model (see Eqs. 53 and 54) using different values of fractal dimension. The results are plotted in Fig. 5. One can see that the relative permeability curves of the nonwetting phase (represented by steam phase in Fig. 3) are almost the same for different values of fractal dimension. However, the relative permeability curves of the wetting phase (represented by water phase in Fig. 5) are different for different values of fractal dimension. The fractal dimension of The Geysers rock is greater than 2.3 (Li and Horne, 2003). Fig. 5 shows that the corresponding relative permeability curves have different features from those with fractal dimension less than 2.0, as predicted by the model (see Eqs. 53 and 54). One can see that the values of the water phase relative permeability for the fractal dimension over 2.3 are very small until the normalized water saturation reaches about 90%. This phenomenon may be verified by future experimental data of steam and water relative permeability measured in The Geysers rock.

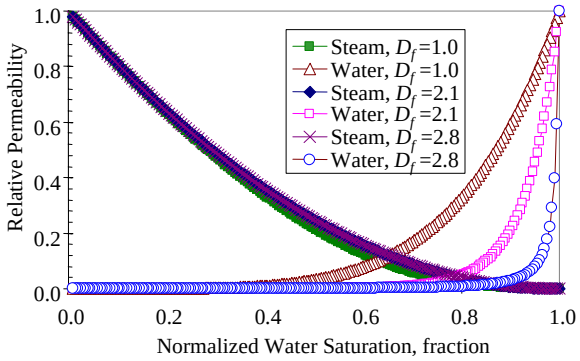

Figure 5: Typical relative permeability curves calculated using the new model with different values of fractal dimension.

The comparison of the experimental steam-water relative permeability in Berea sandstone with the model prediction is shown in Fig. 6. The end-point values of the experimental relative permeability curves were also used as the end-point values of the model relative permeability curves. The experimental steam-water relative permeability data shown in Fig. 6 were measured in the drainage case with the initial water saturation of 100% (Li and Horne, 2001).

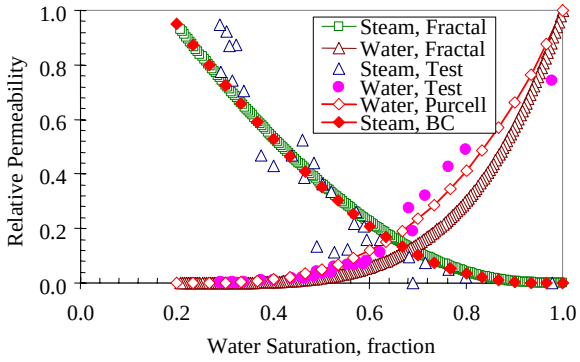

Figure 6: Comparison of experimental with model relative permeability curves.

One can see from Fig. 6 that the model data calculated using the general relative permeability model developed in this study are close to the experimental data once the end-point values are known. Also shown in Fig. 6 is the fit obtained using the Brooks-Corey relative permeability model for the nonwetting phase and using the Purcell relative permeability model for the wetting phase. The reason to use different models for different phases was because we found previously that the Purcell model may be the best fit to the experimental data of the wetting phase relative permeability while the Brooks-Corey model is proposed to calculate the nonwetting phase relative permeability (Li and Horne, 2002).

As mentioned previously, few experimental data of steam-water relative permeability in The Geysers rock have been available in the literature. However Reyes *et al*. (2003) reported the residual water saturation (S_{wr}) with an experimental value of about 70%. The steam relative permeability at S_{wr} is chosen to be equal to 0.6. The water relative permeability at S_{wr} is equal to zero. The end-point values at a water saturation of 100% are known (the water relative permeability is equal to 1.0 and the steam relative permeability is equal to zero). The shape of the relative permeability can be determined using the general relative permeability model with the value of the fractal dimension. Then the steam-water relative permeability curve of The Geysers rock can be obtained and the results are shown in Fig. 7. The value of the fractal dimension chosen was 2.3, which is the typical value of The Geysers rock.

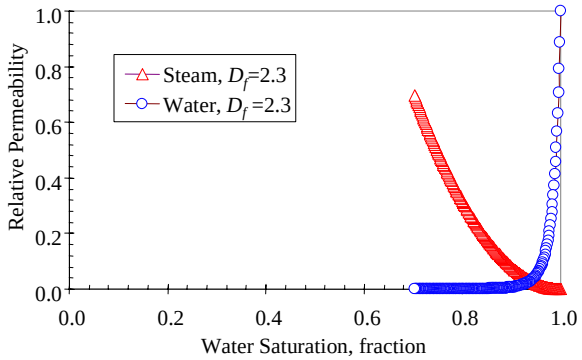

Figure 7: A typical relative permeability curve of The Geysers rock predicted using the general model (Eqs. 49 and 50).

The water phase relative permeability decreases sharply as the water saturation decreases from 100% (see Fig. 7). The speculated explanation is as follows. There are many microfractures in The Geysers rock. In the beginning of the drainage process (the water saturation decreases from 100%), water drains through the microfractures. The water phase relative permeability is great during this period. After the water resided in the microfractures has been drained, the drainage of water in the matrix starts but the flow rate is very low because of the extremely low permeability of the matrix. Accordingly the water phase relative permeability during this period is very small, which forms the sharp drop of the water phase relative permeability as shown in Fig. 7.

It is known that it is difficult to measure steam-water relative permeability because of the mass transfer and the phase transformation as pressure changes. The general relative permeability model derived in this study may facilitate the solution to this problem. Based on the relative permeability model, the shape of the relative permeability curve can be obtained once the capillary pressure curve is known. The capillary pressure curve can be measured easily using a mercury intrusion technique. Therefore the entire steam-water relative permeability curve can be determined once the end-point values are known. This implies that we may only need to measure the end-point values to obtain the entire steam-water relative permeability curve. By doing so, much experimental time and cost can be saved.

CONCLUSION

Based on the present study, the following conclusions may be drawn:

1. Using fractal geometry, a universal model has been developed to represent capillary pressure curves of porous and fractured media.
2. The new capillary pressure model can represent the experimental data of The Geysers rock satisfactorily. However the Brooks-Corey capillary pressure model cannot.
3. The theoretical derivation conducted in this study demonstrated that the Brooks-Corey capillary pressure model may have a solid theoretical base.
4. Relative permeability models for both wetting-phase and nonwetting-phase have been developed accordingly.
5. The relative permeability curves of The Geysers rock may have different features from that of Berea sandstone. For example, the water relative permeability of The Geysers rock may decrease sharply as water saturation decreases.

ACKNOWLEDGMENTS

This research was conducted with financial support to the Stanford Geothermal Program from the US Department of Energy under grant DE-FG07-02ID14418, the contribution of which is gratefully acknowledged.

REFERENCES

Brooks, R.H. and Corey, A.T.: “Hydraulic Properties of Porous Media,” Colorado State University, Hydro paper No.5 (1964).

Burdine, N. T.: "Relative Permeability Calculations from Pore Size Distribution Data", Trans. *AIME*, (1953), 198, 71.

Friesen, W.I. and Mikula, R.J.: “Fractal Dimensions of Coal Particles”, *J. of Colloid and Interface Science*, V. 120, No.1, November 1987.

Li, K. and Horne, R.N.: “An Experimental and Theoretical Study of Steam-Water Capillary Pressure,” *SPEREE* (December 2001), p.477-482.

Li, K. and Horne, R.N.: “Experimental Verification of Methods to Calculate Relative Permeability Using

Capillary Pressure Data," SPE 76757, Proceedings of the 2002 SPE Western Region Meeting/AAPG Pacific Section Joint Meeting held in Anchorage, Alaska, May 20-22, 2002.

Li, K. and Horne, R.N.: "Fractal Characterization of The Geysers Rock," Proceedings of the GRC 2003 annual meeting, October 12-15, 2003, Morelia, Mexico; GRC Trans. V. 27 (2003).

Purcell, W.R.: "Capillary Pressures-Their Measurement Using Mercury and the Calculation of Permeability", Trans. *AIME*, (1949), 186, 39.

Reyes, J.L.P., Li, K., and Horne, R.N.: "Estimating Water Saturation At The Geysers Based On Historical Pressure And Temperature Production Data And By Direct Measurement," Proceedings of the GRC 2003 annual meeting, October 12-15, 2003, Morelia, Mexico; *GRC* Trans. V. **27** (2003).